Magnetoreflectance of films with corrugated surfaces, with magnetic fields applied in the perpendicular configuration

1999 J. Phys.: Condens. Matter 11 1961

(http://iopscience.iop.org/0953-8984/11/8/009)

J. Phys.: Condens. Matter **11** (1999) 1961–1973. Printed in the UK PII: S0953-8984(99)95910-6

Magnetoreflectance of films with corrugated surfaces, with magnetic fields applied in the perpendicular configuration

J H Jacobo-Escobar, G Martínez and Gregorio H Cocoletzi

Instituto de Física, Universidad Autónoma de Puebla, Apartado Postal J-48, Puebla 72570, Mexico

Received 10 July 1998, in final form 11 December 1998

Abstract. The effects of external magnetic $\boldsymbol{B}_0$-fields on the scattering of p-polarized light from metallic films with corrugated surfaces are investigated, with $\boldsymbol{B}_0$ along the growth axis (in the perpendicular configuration). The Rayleigh–Fano and transfer-matrix approaches are applied to obtain $|R_p|^2$ for the scattered fields, with the specular magnetoreflection $|R_0|^2$ displaying minima due to the coupling of the incident light with the surface magnetoplasmons at frequencies in the range $\omega_c < \omega < \omega_H$, where ω_c and ω_H are the cyclotron and hybrid frequencies, respectively, with the gap of the splitting decreasing as the magnetic field strength increases. The presence of a metallic superlattice inhibits the gap between the minima of the surface magnetoplasmon polaritons. In addition, a pseudosurface magnetoplasmon polariton is manifested for both geometries for $\omega < \omega_c$.

1. Introduction

Different techniques have been applied to the study of surface polaritons, attenuated total reflectivity (ATR) [1–3] and scattering of light by rough surfaces [4–6] being two of them, and their combination [7] another one. In the ATR method, a prism of index of refraction $n_p > 1$ is adapted to increase the parallel component of the wave vector to allow the coupling of the incident light with the surface mode. On the other hand, surface roughness may also add momentum to the incident light, producing an excitation of surface polaritons.

Several approaches have been developed to investigate light scattering from rough surfaces for local [8–11] and nonlocal [12–14] media using the Rayleigh–Fano and perturbation theories. In addition, a coordinate transformation has been applied to explore the light scattered from inhomogeneous surfaces [15, 16]. Recent studies [6] of surface plasmon polaritons taking into account the effects of binary metallic superlattices have been carried out on rough surfaces for local media, in which minima of the specular reflectivity and the dispersion relation of the surface plasmon polaritons exhibit a dependence on the surface roughness. One interesting result concerning the surface mode dispersion relation is the appearance of a minigap [11] at a Brillouin zone boundary, which is dependent on the material properties. However, to our knowledge, no magnetic field effects have been considered for systems with rough surfaces. On the other hand, magnetoplasmon polaritons have been studied in semiconductor and metallic media, and in stratified systems of highly doped semiconductors, taking into account an applied magnetic field in the perpendicular [17, 18], Voigt [19, 20], and Faraday [21] geometries. Particular attention has been paid to surface and bulk modes of magnetoplasmons in periodic arrays [22–24]. In the case of periodic superlattices [22, 25, 26] of two alternating highly doped semiconductors, the dispersion relations of surface magnetoplasmons were discussed

0953-8984/99/081961+13$19.50

for the above-mentioned configurations, but no calculations of the optical response have been reported yet.

In this communication, we investigate bulk and surface magnetoplasmons of a metallic film with one surface corrugated and the other flat, and the effects of periodic superlattices composed of alternating metallic and isotropic insulator layers, taking into account an applied magnetic field in the perpendicular configuration—that is, the $\boldsymbol{B}_0$-field is assumed to be directed along the growth axis of the superlattice. The Rayleigh–Fano model [4, 5] and transfer-matrix methods [6, 25, 27, 28] are combined to explore the scattering of p-polarized light incident upon the corrugated surface of the system and the coupling with the surface and bulk magnetoplasmons. The isolated film is first investigated and then the effects of periodic superlattices are considered.

2. Formalism

Let us consider the system depicted in figure 1. The free corrugated surface of the thin film is of thickness $L + \xi(x)$, the frequency- and magnetic-field-dependent dielectric tensor $\tilde{\epsilon}_F(\omega)$ is at $z = L + \xi(x)$, and the region $z < 0$ is filled either with an isotropic insulator of diagonal dielectric tensor ϵ_i (the first case), or a semi-infinite metallic [29] superlattice (the second case) of period $d = d_A + d_B$, where d_A and d_B are the thicknesses, and $\tilde{\epsilon}_A(\omega)$ and $\tilde{\epsilon}_B$ are the dielectric

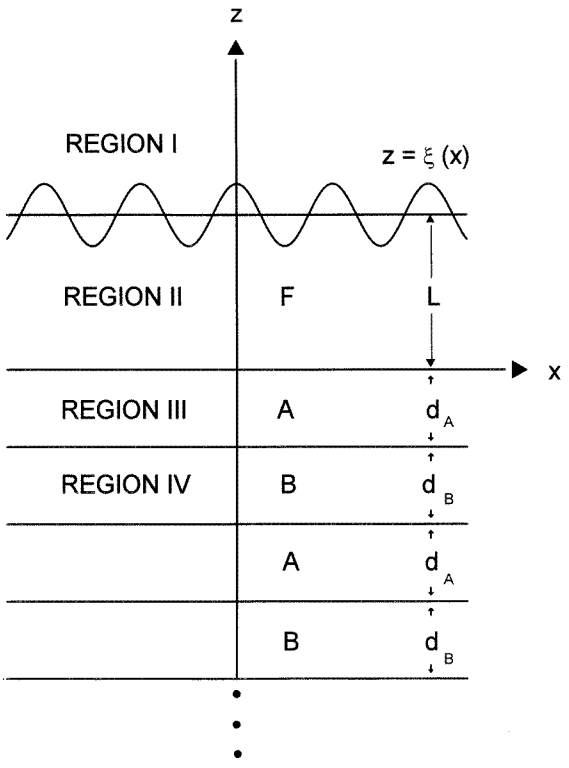

Figure 1. A schematic representation of the thin film with a free corrugated surface, thickness $L + \xi(x)$, and dielectric tensor $\tilde{\epsilon}_F$ in contact with an isotropic insulator of dielectric constant ϵ_i or a semi-infinite superlattice composed of alternating metallic and isotropic insulator layers of thicknesses d_A and d_B, and dielectric tensors $\tilde{\epsilon}_A$ and $\tilde{\epsilon}_B = \tilde{\mathbf{I}}\epsilon_i$, respectively.

tensors of layers A and B, respectively. In due course, one of the layers will be considered as an isotropic insulator with $\tilde{\epsilon} \to \tilde{\mathbf{l}}\epsilon_i$. For the purposes of the present work, the surface profile has the form $\xi(x) = \xi_0 \cos(2\pi/a)x$, where a is the period of the grating. In the perpendicular configuration, the $\boldsymbol{B}_0$-field is directed along the growth axis of the superlattice.

The Maxwell wave equation for a nonisotropic medium has the form

$$\boldsymbol{\nabla} \times (\boldsymbol{\nabla} \times \boldsymbol{E}) - q_0^2 \tilde{\boldsymbol{\epsilon}} \boldsymbol{E} = 0 \tag{1}$$

with plane-wave solutions

$$\boldsymbol{E}(\boldsymbol{r}, t) = \sum_p \boldsymbol{E}_p^0 \mathrm{e}^{\mathrm{i}(\boldsymbol{q}\boldsymbol{r} - \omega t)} \tag{2}$$

where

$$\boldsymbol{q} = (k_p, 0, \beta_p) \qquad k_p = k_x + \frac{2\pi}{a} p \qquad k_x = n q_0 \sin\theta$$

where n is the index of refraction of the isotropic half-space, $q_0 = \omega/c$, and $p = 0, \pm 1, \pm 2, \ldots$. The sum runs from $-\infty$ to $+\infty$, but, in practice, this sum is truncated when searching for convergence, as discussed below. The elements of the dielectric tensor $\tilde{\epsilon}$ are

$$\epsilon_{xx} = \epsilon_{yy} \qquad \epsilon_{yx} = -\epsilon_{xy} \qquad \epsilon_{xz} = \epsilon_{zx} = \epsilon_{yz} = \epsilon_{zy} = 0 \tag{3}$$

and they allow us to rewrite equation (1) in the form

$$\begin{pmatrix} \beta_p^2 - q_0^2\epsilon_{xx} & -q_0^2\epsilon_{xy} & -k_p\beta_p \\ q_0^2\epsilon_{yx} & -(q^2 - q_0^2\epsilon_{xx}) & 0 \\ k_p\beta_p & 0 & -(k_p^2 - q_0^2\epsilon_{zz}) \end{pmatrix} \begin{pmatrix} E_x \\ E_y \\ E_z \end{pmatrix} = 0. \tag{4}$$

This set of linear homogeneous equations have nontrivial solutions when the determinant of the system vanishes, which in turn yields

$$-\beta_p^2 = \frac{1}{2\epsilon_{zz}} \left[k_p^2(\epsilon_{xx} + \epsilon_{zz}) \pm \sqrt{k_p^4(\epsilon_{xx} - \epsilon_{zz})^2 + 4\Lambda^2 q_0^2 \epsilon_{yx}^2 \epsilon_{zz}} \right] \tag{5}$$

where $\Lambda^2 = k_p^2 - q_0^2\epsilon_{zz}$. If β_p is real, there is bulk mode propagation, but if it is imaginary, there is surface mode localization.

The components of the electromagnetic fields in the rough film are expressed as

$$E_x^F = \sum_p \mathrm{e}^{\mathrm{i}k_p x} (E_p^+ \mathrm{e}^{\mathrm{i}\beta_{p1}z} + E_p^- \mathrm{e}^{-\mathrm{i}\beta_{p1}z} + F_p^+ \mathrm{e}^{\mathrm{i}\beta_{p2}z} + F_p^- \mathrm{e}^{-\mathrm{i}\beta_{p2}z}) \tag{6}$$

$$B_y^F = \sum_p \frac{\gamma_p}{q_0} \mathrm{e}^{\mathrm{i}k_p x} (\beta_{p1} E_p^+ \mathrm{e}^{\mathrm{i}\beta_{p1}z} - \beta_{p1} E_p^- \mathrm{e}^{-\mathrm{i}\beta_{p1}z} + \beta_{p2} F_p^+ \mathrm{e}^{\mathrm{i}\beta_{p2}z} - \beta_{p2} F_p^- \mathrm{e}^{-\mathrm{i}\beta_{p2}z}) \tag{7}$$

$$E_y^F = \sum_p \mathrm{e}^{\mathrm{i}k_p x} (\delta_{p1} E_p^+ \mathrm{e}^{\mathrm{i}\beta_{p1}z} + \delta_{p1} E_p^- \mathrm{e}^{-\mathrm{i}\beta_{p1}z} + \delta_{p2} F_p^+ \mathrm{e}^{\mathrm{i}\beta_{p2}z} + \delta_{p2} F_p^- \mathrm{e}^{\mathrm{i}\beta_{p2}z}) \tag{8}$$

$$B_x^F = -\frac{1}{q_0} \sum_p \mathrm{e}^{\mathrm{i}k_p x} (\beta_{p1}\delta_{p1} E_p^+ \mathrm{e}^{\mathrm{i}\beta_{p1}z} - \beta_{p1}\delta_{p1} E_p^- \mathrm{e}^{-\mathrm{i}\beta_{p1}z} + \beta_{p2}\delta_{p2} F_p^+ \mathrm{e}^{\mathrm{i}\beta_{p2}z} - \beta_{p2}\delta_{p2} F_p^- \mathrm{e}^{\mathrm{i}\beta_{p2}z}) \tag{9}$$

where we have used the expressions

$$B_{yp} = \frac{\gamma_p \beta_p}{q_0} E_{xp} \qquad E_{zp} = \gamma_p' E_{xp}$$

which are obtained from equation (4) with

$$\gamma_p = -\frac{q_0^2\epsilon_{zz}}{k_p^2 - q_0^2\epsilon_{zz}} \qquad \gamma_p' = -\frac{k_p\beta_p}{q_0^2\epsilon_{zz}}\gamma_p \qquad \delta_{pi} = \frac{q_0^2\epsilon_{yx}}{k_i^2 - q_0^2\epsilon_{xx}}.$$

For region I, we write $\boldsymbol{B} = (0, B_y^v, 0)\mathrm{e}^{-\mathrm{i}\omega t}$ and $\boldsymbol{E} = (E_x^v, 0, E_z^v)\mathrm{e}^{-\mathrm{i}\omega t}$ with

$$B_y^v = \mathrm{e}^{\mathrm{i}(k_0 x - \alpha_{0v} z)} + \sum_p R_p \mathrm{e}^{\mathrm{i}(k_p x + \alpha_{pv} z)}. \tag{10}$$

The first term corresponds to the incident field, and the second to the scattered field. For an isotropic transparent insulator filling the space $z < 0$, there are only transmitted waves; therefore, we write

$$B_y^T = \sum_p T_p \mathrm{e}^{\mathrm{i}(k_p x - \alpha_{pv} z)} \tag{11}$$

where $\alpha_{pv}^2 = q_0^2 - k_p^2$. To obtain E_x, we use the relation

$$E_x = -\frac{\mathrm{i}}{q_0}\frac{\partial B_y}{\partial z}.$$

To solve for the scattered amplitudes of the electromagnetic fields, we first write out Maxwell boundary conditions: the continuity of the tangential components of the electric field $\boldsymbol{E}_t$ and the magnetic field $\boldsymbol{B}_t$ gives

$$\boldsymbol{E}_t = \boldsymbol{E} - (\hat{\boldsymbol{n}} \cdot \boldsymbol{E})\hat{\boldsymbol{n}} \tag{12}$$

$$\boldsymbol{B}_t = \boldsymbol{B} - (\hat{\boldsymbol{n}} \cdot \boldsymbol{B})\hat{\boldsymbol{n}} \tag{13}$$

at $z = 0$ and $z = L + \xi(x)$. To define the unit vector $\hat{\boldsymbol{n}}$, let $\phi = c$ describe an arbitrary surface; then the outward-normal unit vector $\hat{\boldsymbol{n}}$ is expressed as

$$\hat{\boldsymbol{n}} = \frac{\boldsymbol{\nabla}\phi}{|\boldsymbol{\nabla}\phi|}. \tag{14}$$

For $\phi = z - \xi(x)$, where $\xi(x)$ is the surface profile, we have

$$\hat{\boldsymbol{n}} = (-\hat{\boldsymbol{i}}\xi' + \hat{\boldsymbol{k}})/[1 + (\xi')^2]^{1/2}. \tag{15}$$

We therefore obtain

$$E_{tx} = -[1 + (\xi')^2]^{-1}\left[\epsilon E_x + \frac{\epsilon_{xy}}{\epsilon_{zz}}E_y + \frac{\mathrm{i}}{q_0\epsilon_{zz}}\left(-\xi'\frac{\partial}{\partial x} + \frac{\partial}{\partial z}\right)B_y\right]. \tag{16}$$

Here $\epsilon = (\epsilon_{xx} - \epsilon_{zz})/\epsilon_{zz}$. Applying boundary conditions (12) and (13), and after some algebraic manipulation [4–6], we get

$$\sum_p \begin{pmatrix} M_{lp}^{(11)} & M_{lp}^{(12)} \\ M_{lp}^{(21)} & M_{lp}^{(22)} \end{pmatrix} \begin{pmatrix} R_p \\ T_p \end{pmatrix} = \begin{pmatrix} V_l \\ W_l \end{pmatrix} \tag{17}$$

where the matrix elements are

$$M_{lp}^{(11)} = \mathrm{i}^{l-p}\mathrm{e}^{\mathrm{i}\alpha_{pv}L} J_{l-p}(\alpha_{pv}\xi_0) \tag{18}$$

$$\begin{aligned} M_{lp}^{(12)} = {} & -\frac{\gamma_p}{q_0}\beta_{p1}[S_{p1}\mathrm{i}^{l-p}\mathrm{e}^{\mathrm{i}\beta_{p1}L} - S_{p2}(-\mathrm{i})^{l-p}\mathrm{e}^{-\mathrm{i}\beta_{p1}L}]J_{l-p}(\beta_{p1}\xi_0) \\ & - \frac{\gamma_p}{q_0}\beta_{p2}[S_{p3}\mathrm{i}^{l-p}\mathrm{e}^{\mathrm{i}\beta_{p2}L} - (-\mathrm{i})^{l-p}S_{p4}\mathrm{e}^{-(\mathrm{i}\beta_{p2}L)}]J_{l-p}(\beta_{p2}\xi_0) \end{aligned} \tag{19}$$

$$M_{lp}^{(21)} = \mathrm{i}^{l-p}\left(\frac{q_0^2 - k_p k_l}{q_0\alpha_{pv}}\right)\mathrm{e}^{\mathrm{i}\alpha_{pv}L} J_{l-p}(\alpha_{pv}\xi_0) \tag{20}$$

$$\begin{aligned} M_{lp}^{(22)} = {} & \epsilon_{1lp}[\mathrm{i}^{l-p}S_{p1}\mathrm{e}^{\mathrm{i}\beta_{p1}L} + (-\mathrm{i})^{l-p}S_{p2}\mathrm{e}^{-\mathrm{i}\beta_{p1}L}]J_{l-p}(\beta_{p1}\xi_0) \\ & + \epsilon_{2lp}[\mathrm{i}^{l-p}S_{p3}\mathrm{e}^{\mathrm{i}\beta_{p2}L} + (-\mathrm{i})^{l-p}S_{p4}\mathrm{e}^{-\mathrm{i}\beta_{p2}L}]J_{l-p}(\beta_{p2}\xi_0) \end{aligned} \tag{21}$$

$$V_l = -(-\mathrm{i})^l \mathrm{e}^{-\mathrm{i}\alpha_{0v}L} J_l(\alpha_{0v}\xi_0) \tag{22}$$

$$W_l = (-\mathrm{i})^l \frac{q_0^2 - k_0 k_l}{q_0 \alpha_{0v}} \mathrm{e}^{-\mathrm{i}\alpha_{0v}L} J_l(\alpha_{0v}\xi_0). \tag{23}$$

In the expression for $M_{lp}^{(22)}$, the coefficients ϵ_{1lp} and ϵ_{2lp} have the form

$$\epsilon_{1lp,2lp} = \epsilon + \frac{\epsilon_{xy}}{\epsilon_{zz}}\delta_{p1,2} - \frac{\gamma_p}{q_0^2 \epsilon_{zz}}(\beta_{p1,2} - k_p(k_p - k_l)). \tag{24}$$

In these equations, $J_k(\beta_{pi}\xi_0)$ are Bessel functions of the second kind. The coefficients S_{pi} are defined below.

Equations (17) are the reduced Rayleigh equations that have to be solved for R_p and T_p, restricting l and p to taking values of a convergence index N, i.e. l, p must take the values $0, \pm 1, \pm 2, \ldots, \pm N$. In our case, convergence was achieved with $N = 3$.

In the second case we deal with the space $z < 0$ filled with a [30] semi-infinite superlattice constructed of metallic and isotropic insulator layers, as depicted in figure 1. Let us describe the procedure used to construct the transfer matrices. For the isotropic insulator, we write

$$B_y^{\mathrm{A}} = \sum_p \mathrm{e}^{\mathrm{i}k_p x}(G_1 \mathrm{e}^{\mathrm{i}\alpha_{pv}z} + G_2 \mathrm{e}^{-\mathrm{i}\alpha_{pv}z}) \tag{25}$$

$$E_x^{\mathrm{A}} = \frac{1}{q_0}\sum_p \alpha_{pv}\mathrm{e}^{\mathrm{i}k_p x}(G_1 \mathrm{e}^{\mathrm{i}\alpha_{pv}z} - G_2 \mathrm{e}^{-\mathrm{i}\alpha_{pv}z}). \tag{26}$$

Following a familiar procedure [6], we obtain

$$\begin{pmatrix} E_x^{\mathrm{A}} \\ B_y^{\mathrm{A}} \end{pmatrix}_{z^u} = \sum_p \mathbf{M}_p^{\mathrm{A}} \int \mathrm{d}x'\, \mathrm{e}^{\mathrm{i}k_p(x-x')} \begin{pmatrix} E_x^{\mathrm{A}} \\ B_y^{\mathrm{A}} \end{pmatrix}_{z^l} \tag{27}$$

where z^u and z^l stand for the upper and lower boundaries of an air gap, respectively, and the transfer matrix has the form

$$\mathbf{M}_p^{\mathrm{A}} = \begin{pmatrix} \cos\alpha_{pv}d_{\mathrm{A}} & \mathrm{i}\dfrac{\omega}{c\alpha_{pv}}\sin\alpha_{pv}d_{\mathrm{A}} \\ \mathrm{i}\dfrac{c\alpha_{pv}}{\omega}\sin\alpha_{pv}d_{\mathrm{A}} & \cos\alpha_{pv}d_{\mathrm{A}} \end{pmatrix}. \tag{28}$$

In a metallic layer there are four travelling waves, two moving down and two up. We use the tangential components of $\boldsymbol{E}$ and $\boldsymbol{B}$, namely E_v and B_v, where $v = x, y$, to construct the transfer matrix. Following reference [6] we obtain

$$\begin{pmatrix} \boldsymbol{E}^{\mathrm{B}} \\ \boldsymbol{B}^{\mathrm{B}} \end{pmatrix}_{z^d} = \sum_p \mathbf{M}_p^{\mathrm{B}} \int \mathrm{d}x''\, \mathrm{e}^{\mathrm{i}k_l(x'-x'')} \begin{pmatrix} \boldsymbol{E}^{\mathrm{B}} \\ \boldsymbol{B}^{\mathrm{B}} \end{pmatrix}_{z^i} \tag{29}$$

where $\mathbf{M}_p^{\mathrm{B}} = \mathbf{G}_p^{\mathrm{B}}\mathbf{T}(d_{\mathrm{B}})(\mathbf{G}_p^{\mathrm{B}})^{-1}$, with

$$\mathbf{G}_p^{\mathrm{B}} = \begin{pmatrix} 1 & 1 & 1 & 1 \\ \delta_{p1}^{\mathrm{B}} & \delta_{p1}^{\mathrm{B}} & \delta_{p2}^{\mathrm{B}} & \delta_{p2}^{\mathrm{B}} \\ -\dfrac{\beta_{p1}^{\mathrm{B}}\delta_{p1}^{\mathrm{B}}}{q_0} & \dfrac{\beta_{p1}^{\mathrm{B}}\delta_{p1}^{\mathrm{B}}}{q_0} & -\dfrac{\beta_{p2}^{\mathrm{B}}\delta_{p2}^{\mathrm{B}}}{q_0} & \dfrac{\beta_{p2}^{\mathrm{B}}\delta_{p2}^{\mathrm{B}}}{q_0} \\ \dfrac{\beta_{p1}^{\mathrm{B}}\gamma_p^{\mathrm{B}}}{q_0} & -\dfrac{\beta_{p1}^{\mathrm{B}}\gamma_p^{\mathrm{B}}}{q_0} & \dfrac{\beta_{p2}^{\mathrm{B}}\gamma_p^{\mathrm{B}}}{q_0} & -\dfrac{\beta_{p2}^{\mathrm{B}}\gamma_p^{\mathrm{B}}}{q_0} \end{pmatrix} \tag{30}$$

and

$$\mathbf{T}(d_{\mathrm{B}}) = \mathrm{diag}(\mathrm{e}^{\mathrm{i}\beta_{p1}^{\mathrm{B}}d_{\mathrm{B}}}, \mathrm{e}^{-\mathrm{i}\beta_{p1}^{\mathrm{B}}d_{\mathrm{B}}}, \mathrm{e}^{\mathrm{i}\beta_{p2}^{\mathrm{B}}d_{\mathrm{B}}}, \mathrm{e}^{-\mathrm{i}\beta_{p2}^{\mathrm{B}}d_{\mathrm{B}}}).$$

Then the matrix elements of $\mathbf{M}_p$ are

$$M_{11} = (\delta_{p2}c_1 - \delta_{p1}c_2)/\Delta_1 \qquad M_{12} = (-c_1 + c_2)/\Delta_1 \tag{31}$$

$$M_{13} = q_0\left(\frac{s_1}{\alpha_{p1}} - \frac{s_2}{\alpha_{p2}}\right)\Big/\gamma_p\Delta_1 \qquad M_{14} = q_0\left(\frac{\delta_{p2}}{\alpha_{p1}}s_1 - \frac{\delta_{p1}}{\alpha_{p2}}s_2\right)\Big/\gamma_p\Delta_1 \tag{32}$$

$$M_{21} = \delta_{p1}\delta_{p2}(c_1 - c_2)/\Delta_1 \qquad M_{22} = (-\delta_{p1}c_1 + \delta_{p2}c_2)/\Delta_1 \tag{33}$$

$$M_{23} = q_0\left(\frac{\delta_{p1}}{\alpha_{p1}}s_1 - \frac{\delta_{p2}}{\alpha_{p2}}s_2\right)\Big/\Delta_1 \qquad M_{24} = q_0\delta_{p1}\delta_{p2}\left(\frac{s_1}{\alpha_{p1}} - \frac{s_2}{\alpha_{p2}}\right)\Big/\Delta_1 \tag{34}$$

$$M_{31} = \delta_{p1}\delta_{p2}(-\alpha_{p1}s_1 + \alpha_{p2}s_2)/\Delta_1 \qquad M_{32} = (\delta_{p1}\alpha_{p1}s_1 - \delta_{p2}\alpha_{p2}s_2)/q_0\Delta_1 \tag{35}$$

$$M_{33} = (-\delta_{p1}c_1 + \delta_{p2}c_2)/\Delta_1 \qquad M_{34} = \delta_{p1}\delta_{p2}(-c_1 + c_2)/\Delta_1 \tag{36}$$

$$M_{41} = \gamma_p(\delta_{p2}\alpha_{p1}s_1 - \delta_{p1}\alpha_{p2}s_2)/\Delta_1 \qquad M_{42} = \gamma_p(-\alpha_{p1}s_1 + \alpha_{p2}s_2)/q_0\Delta_1 \tag{37}$$

$$M_{43} = \gamma_p(c_1 - c_2)/\Delta_1 \qquad M_{44} = (\delta_{p2}c_1 - \delta_{p1}c_2)/\Delta_1 \tag{38}$$

where $\Delta_1 = \delta_{p2} - \delta_{p1}$, $c_i = \cos(\alpha_{pi}d)$, and $s_i = \sin(\alpha_{pi}d)$, with $i = 1, 2$.

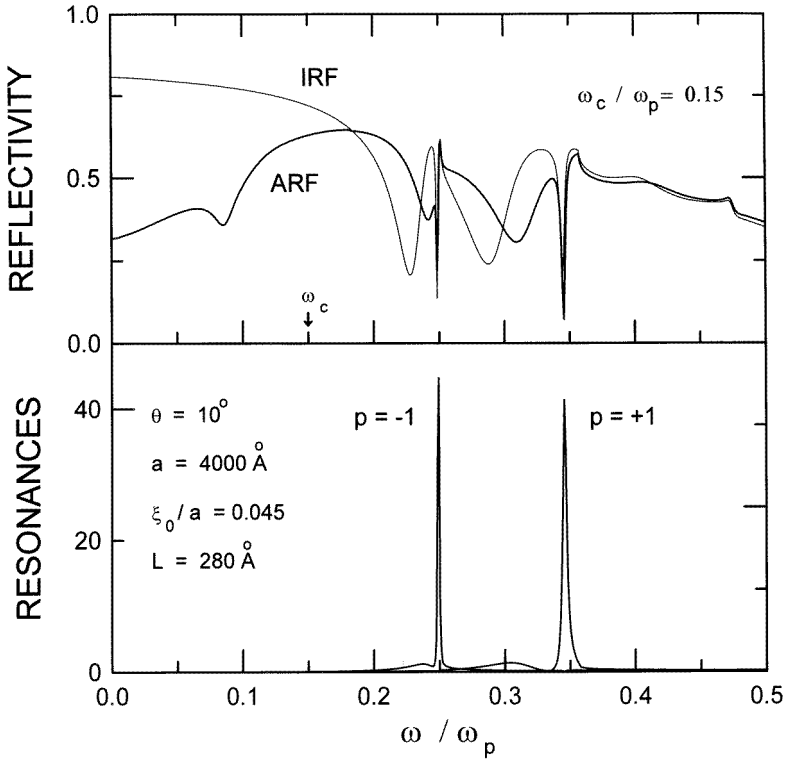

Figure 2. Results for the p-polarized specular reflectivity (upper panel) for $\theta = 10^\circ$, $a = 4000$ Å, $L = 380$ Å, and $\zeta_0/a = 0.0, 0.045$. The thick curve corresponds to the ARF system and takes into account an external $\boldsymbol{B}_0$-field ($\omega_c/\omega_p = 0.15$) while the thin line is for the IRF system with no external field. The resonances R_{+1} and R_{-1} are displayed in the lower panel, taking into account a $\boldsymbol{B}_0$-field as in the upper panel.

It is noted that the transfer matrix of a metallic layer is of dimension 4×4 [27,28], but for the insulator layer it is of dimension 2×2; therefore, boundary conditions cannot be applied to them as they stand. To obtain the total matrix, we collapse [27,28] the 4×4 transfer matrix into a 2×2 matrix with the use of $E_y^{\mathrm{A}} = B_x^{\mathrm{A}} = 0$ evaluated at the layer surfaces, and then apply boundary conditions. The result is cast into the form

$$\begin{pmatrix} E_x^{\mathrm{A}} \\ B_y^{\mathrm{A}} \end{pmatrix}_{z^d} (x) = \mathbf{M} \begin{pmatrix} E_x^{\mathrm{B}} \\ B_y^{\mathrm{B}} \end{pmatrix}_{z^i} (x) \tag{39}$$

where $\mathbf{M} = \mathbf{M}_p^{\mathrm{A}} \mathbf{M}_p^{\mathrm{B}}$. For a periodic system with period $d = d_a + d_{\mathrm{B}}$, Bloch's theorem may be combined with equation (39) to give

$$\mathbf{M} \begin{pmatrix} E_x^{\mathrm{A}} \\ B_y^{\mathrm{A}} \end{pmatrix}_{z+d} (x) = \mathrm{e}^{\mathrm{i}qd} \begin{pmatrix} E_x^{\mathrm{A}} \\ B_y^{\mathrm{A}} \end{pmatrix}_{z+d} (x). \tag{40}$$

In this equation, q is the one-dimensional Bloch wave vector.

In order to calculate $G_1/G_2 = S_p$, we consider

$$\begin{pmatrix} E_x^{\mathrm{A}} \\ B_y^{\mathrm{A}} \end{pmatrix}_z (x) = \sum_p \mathrm{e}^{\mathrm{i}k_p x} G_p^{\mathrm{A}} \begin{pmatrix} G_1 \\ G_2 \end{pmatrix}_z (x) \tag{41}$$

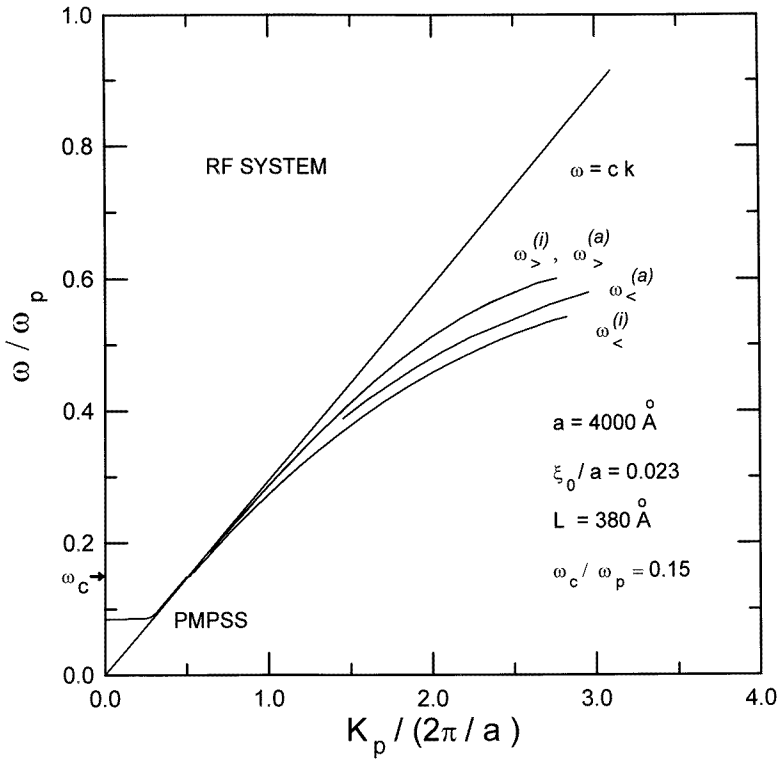

Figure 3. Dispersion relations of surface and pseudosurface modes for the RF system. The curves labelled with $\omega_<^i$ and $\omega_>^i$ are with no applied field while the ones labelled with $\omega_<^a$ and $\omega_>^a$ were obtained taking into account a $\boldsymbol{B}_0$-field, and $\omega_c/\omega_p = 0.15$. Recall that the pseudosurface polaritons are located on the left of the light line. The other parameters are indicated in the figure.

from which we obtain

$$S_p = \frac{(M_{11} + M_{21}) + (q_0/\alpha_{pv})(M_{12} + M_{22}) - (1 + q_0/\alpha_{pv})\mathrm{e}^{-\mathrm{i}pd}}{-(M_{11} + M_{21}) + (q_0/\alpha_{pv})(M_{12} + M_{22)} + (1 - q_0/\alpha_{pv})\mathrm{e}^{-\mathrm{i}pd}}. \tag{42}$$

In this report, the specular reflectance and magnetoreflectance $|R_0|^2$, the first-order resonances $|R_{\pm 1}|^2$, and the dispersion relations of surface plasmon and magetoplasmon polaritons are investigated. These studies are carried out by solving numerically Rayleigh equations (17).

3. Results and discussion

Numerical calculations are presented for local corrugated metallic films—firstly, considering the isolated film and secondly, the film in contact with a local metallic superlattice. The nonzero elements of the metallic dielectric tensor have the forms

$$\epsilon_{xx} = \epsilon_\infty \left[1 - \frac{\omega_p^2}{\omega} \left[\frac{\omega + \mathrm{i}\tau}{(\omega + \mathrm{i}\tau)^2 - \omega_c^2} \right] \right] \tag{43}$$

$$\epsilon_{xy} = -\epsilon_{yx} = \epsilon_\infty \left[\mathrm{i} \frac{\omega_c}{\omega} \frac{\omega_p^2}{(\omega + \mathrm{i}\tau)^2 - \omega_c^2} \right] \tag{44}$$

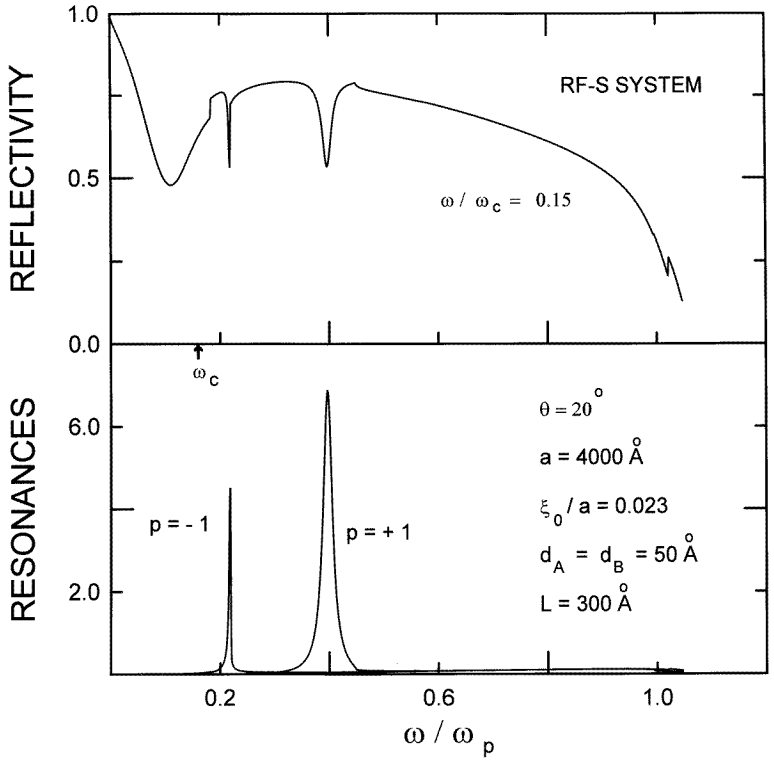

Figure 4. This figure displays the specular reflectivity (upper panel) and the resonances (lower panel) in the presence of an external magnetic field of a corrugated film in contact with a semi-infinite superlattice (the RF–S system) composed of alternating metallic layers with Drude dielectric functions and isotropic insulator layers with frequency-independent dielectric functions ($\epsilon_i = 1.2$). $\omega_c/\omega_p = 0.15$, and the other parameters are shown in the figure.

$$\epsilon_{zz} = \epsilon_\infty \left[1 - \frac{\omega_p^2}{\omega(\omega + i\tau)} \right] \tag{45}$$

where ω_c and ω_p are the cyclotron and plasma frequencies. In our work, we consider the case of magnesium; then $\epsilon_\infty = 1$, $\hbar\omega_p = 10.5$ eV, and $\tau\omega_p = 0.06$ [29]. For most of the cases presented, $\omega_c = 0.15\,\omega_p$ and the grating period $a = 4000$ Å. The z-components of the wave vector β_i $(i = 1, 2)$ may take values which are imaginary, real, complex, or one real and the other imaginary to produce bulk, surface, complex, or pseudosurface modes [3, 18, 22], respectively.

Figure 2 shows results for isolated films. In the upper panel, the reflectivity $|R_0|^2$ is displayed for an angle of incidence of 10°, $\xi_0/a = 0.045$, and $L = 380$ Å. At frequencies $\omega < \omega_c$, the curve with no magnetic field (the IRF system) shows no structure; in contrast, the one with an applied field (the ARF system) displays a minimum originating from a pseudosurface magnetoplasmon. For the region $\omega_c < \omega < \omega_H < \omega_p$, where $\omega_H = [\frac{1}{2}(\omega_c^2 + \omega_p^2)]^{1/2}$ is the critical frequency [31], that plays the role of an upper limit for the surface modes. The curve with no magnetic field exhibits two pairs of minima produced by the splitting of the $|R_0|^2$ minima due to the coupling of the incident light with the antisymmetric and symmetric modes of the flat film, respectively—that is, a surface corrugation effect. The two minima at lower frequency were obtained with $p = -1$ while the other two at higher frequencies correspond to $p = +1$. When a magnetic field is applied, yielding $\omega_c = 0.15\,\omega_p$, the gap of the splitting

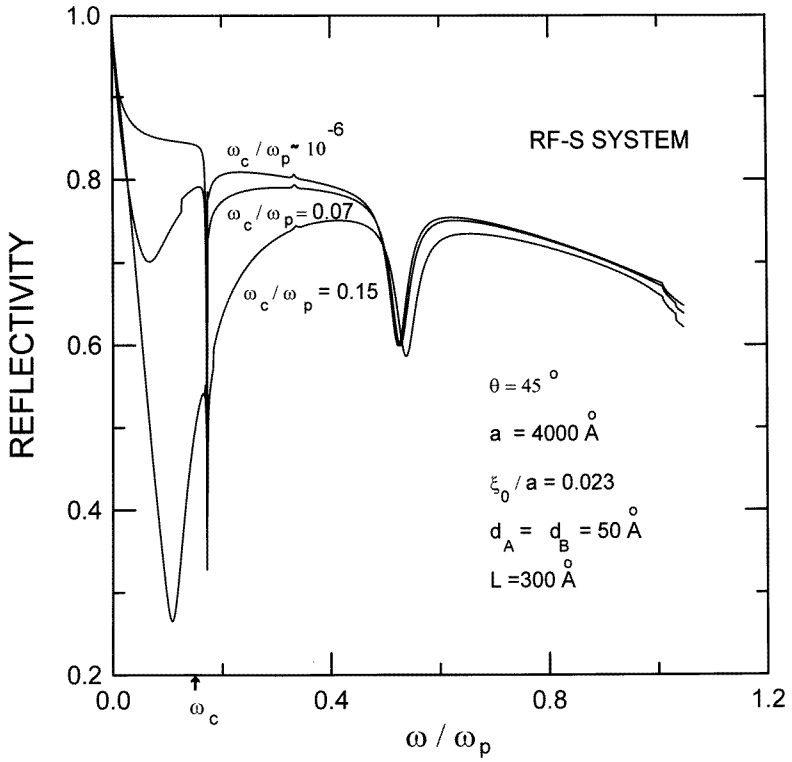

Figure 5. The specular reflectivity of a film in contact with a superlattice (the RF–S system) made up of alternating metallic and isotropic insulator ($\epsilon_i = 1.2$) layers for different magnetic field strengths with the parameters shown in the figure.

decreases and at the same time the broad minima become less deep. To complement the discussion on the coupling of the incident light with the surface modes, we calculated the resonances for $p = \pm 1$ taking into account an external magnetic field, as shown in the lower panel. Two sharp peaks were obtained corresponding to the two deepest minima of $|R_0|^2$, and two smaller shoulders which are at the positions of the broad minima of the specular reflection. We interpret sharp resonances as indicating strong coupling and broad resonances as indicating weak coupling with the incident light. Resonances in the absence of applied external fields show a similar behaviour to that in the presence of $\boldsymbol{B}$-fields. It is important to remark that pseudosurface modes exhibit no resonances with these parameters.

Using the formula $K_p = (2\pi/a)k_p$, where $k_p = n(\omega_{min}/c)\sin\theta \pm p\,2\pi/a$ and ω_{min} is the frequency of the minima of $|R_0|^2$, calculations were performed for the 'optical' dispersion relations of surface plasmons and magnetoplasmons, for corrugated films (the RF system). Here we took $n = 1$, as vacuum is considered to fill the upper half-space, anticipating that no qualitative changes would be obtained if one set $n > 1$. The results are shown in figure 3, where $\omega^i_>$ and $\omega^a_>$ stand for the upper branch without and with applied external fields, and $\omega^i_<$ and $\omega^a_<$ label the lower branch without and with $\boldsymbol{B}$-fields, respectively. The light line $\omega = ck$ is also shown. $\omega_c = 0.15\ \omega_p$, $\xi_0 = 0.023\ a$, and $L = 380$ Å. As stated before, the applied field closes the gap of the splitting of the minima; therefore this induces no separation between the dispersion relation curves, as depicted in the figure. On the other hand, with no magnetic

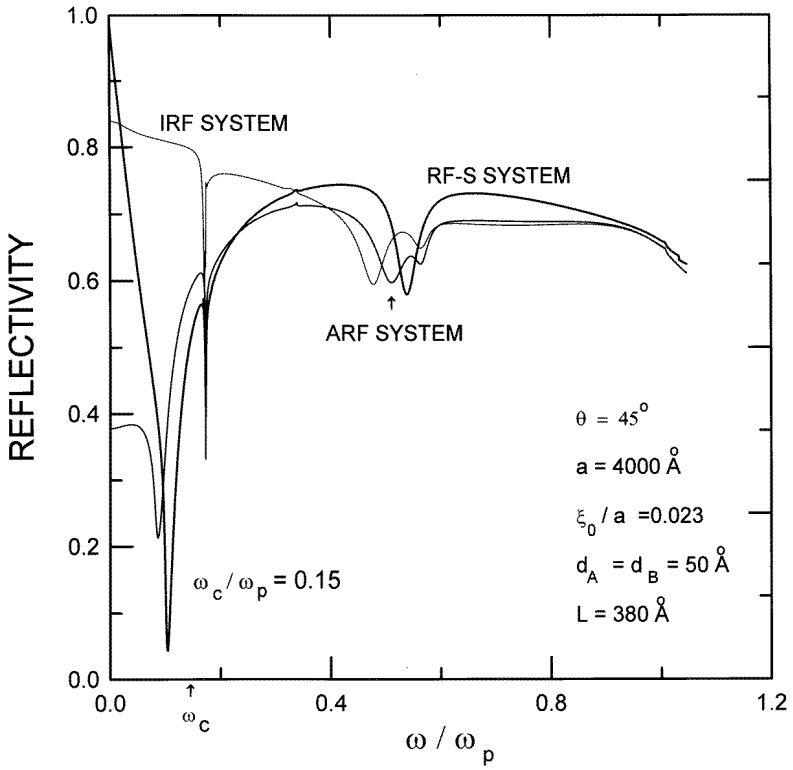

Figure 6. Comparison of the specular magnetoreflectivities of three different systems: an isolated film (IRF system) with no applied field, an isolated film (ARF system) with an external field, and a film in contact with a superlattice (the RF–S system). The parameters are as shown.

field, the dispersion relations of the surface plasmons are well separated, as indicated by the larger gap between the minima. The pseudosurface modes lie on the left of the light line; consequently, this cannot be observed experimentally.

The reflectivity and resonances are shown in figure 4 for a rough film in contact with a superlattice (the RF–S system) formed of alternating metallic and isotropic insulator layers. As it is quite unimportant, and for simplicity, we set $\epsilon_i = 1.2$. In fact, calculations with $\epsilon_i = 1$ have been performed that exhibit no qualitative differences from those reported here. In the upper panel we display $|R_0|^2$, where two minima are manifested due to the coupling of the incident light with the surface magnetoplasmon and there is an additional minimum as a consequence of the pseudosurface magnetoplasmon presence. In the lower panel, $|R_{\pm 1}|^2$ are exhibited with the resonances corresponding to the frequencies of the surface polaritons. It is noted that no splitting of the minima appears, as in the case of an isolated rough film; that is, the superlattice inhibits the gaps, and in addition, enhances the pseudosurface plasmon minimum.

The effects of different choices of magnetic field strengths on the specular reflectivity are presented in figure 5 taking into account the presence of the metallic superlattice (the RF–S system). The parameters are; $\theta = 45^\circ$, $\xi_0 = 0.023\,a$, $L_A = L_B = 50$ Å, $L = 300$ Å. The cyclotron frequency decreases with $\boldsymbol{B}_0$, producing a shift of the resonances towards lower energies. The depths of the minima are affected by these variations—since they correspond to

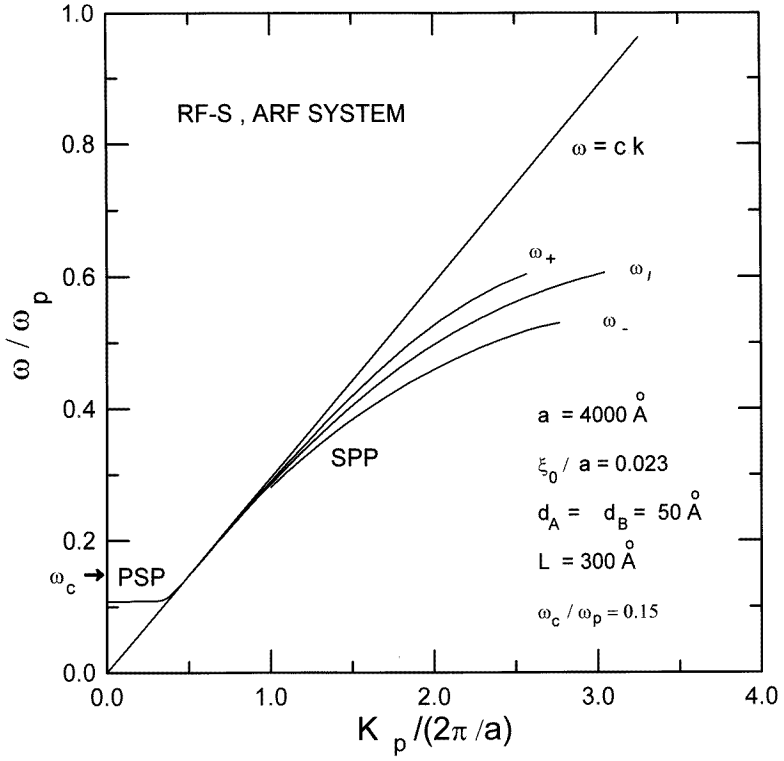

Figure 7. Comparison of the surface plasmon polariton (SPP) dispersion relation curves for an isolated film—curves labelled with $\omega_{+,-}$—and a film in contact with a metallic superlattice—the curve labelled with ω_l—taking into account an external field. The parameters are shown in the figure.

the pseudosurface mode, they are the most sensitive to the changes.

Specular reflectivity variations as functions of the geometries are depicted in figure 6 where the parameters have the following values: $\theta = 45^{\circ}$, $L_{\mathrm{A}} = L_{\mathrm{B}} = 50$ Å, and $L = 380$ Å. As described above, the minima of the surface plasmons and magnetoplasmons show a split induced by the roughness, and the gap between them decreases as the magnetic field strength increases. These effects can be observed by comparing the curves labelled 'ARF system' (the rough film with an applied field) and 'IRF system' (the rough film without a $\boldsymbol{B}_0$-field). On the other hand, results for the reflectivity for a system taking into account the presence of the superlattice exhibit no gap and an enhanced minimum associated with the pseudosurface magnetoplasmons: see the curve labelled 'RF–S system'.

In figure 7 we compare the dispersion relations of the surface magnetoplasmons of the isolated rough film (the ARF curve) and the rough film in contact with the metallic superlattice (the RF–S curve). For this figure $\xi_0 = 0.023\ a$, $L_{\mathrm{A}} = L_{\mathrm{B}} = 50$ Å, $L = 300$ Å, and $\omega_c = 0.15\ \omega_p$. Curves for the surface modes corresponding to the ARF system (labelled with $\omega_{\pm}$) are consequences of the splitting, while that for the RF–S system lies between those labelled ω_{-} and ω_{+}. We have included results for the pseudosurface modes appearing below the cyclotron frequency and to the left of the light line.

In conclusion, we have presented a study of the optical properties of plasmon and magnetoplasmon polaritons of corrugated metallic films and corrugated metallic films in contact with semi-infinite metallic superlattices taking into account an applied magnetic field in the perpendicular configuration. The Rayleigh–Fano model and 4×4 transfer-matrix approaches have been used to calculate the specular reflectivity $|R_0|^2$, resonances $|R_{\pm}|^2$, and dispersion relation of the surface plasmons and magnetoplasmon polaritons. The results exhibit a dependence on the surface corrugation as well as on the magnetic field strength. The specular reflectivity of the isolated corrugated film shows splittings of the minima due to the coupling of light with the surface modes, corresponding to the antisymmetric and symmetric flat-film surface waves, as produced by the nonhomogeneity of the surface, with the gap between two minima decreasing as the $\boldsymbol{B}_0$-field increases. On the other hand, the presence of the metallic superlattices inhibits the splitting of the minima of the flat-film antisymmetric and symmetric modes.

Acknowledgment

This work was partially supported by CONACyT-México, grant No 26363-E.

References

[1] Otto A 1968 *Z. Phys.* **216** 398
Kretschmann E and Raether H 1968 *Z. Naturf.* a **23** 2135
Kretschmann E 1971 *Z. Phys.* **241** 313
[2] Palik E D, Kaplan R, Gamow R W, Kaplan H, Wallis R F and Quinn J J 1976 *Phys. Rev.* B **13** 2497
[3] Boardman A D (ed) 1982 *Electromagnetic Surface Modes* (New York: Wiley)
[4] Cavalcante M G, Farías G A and Maradudin A A 1987 *J. Opt. Soc. Am.* B **4** 1372
[5] Crego C R and Rustgi M L 1990 *J. Opt. Soc. Am.* B **7** 877
[6] Jacobo-Escobar J H, Saldaña X I and Cocoletzi G H 1998 *J. Phys.: Condens. Matter* **10** 5807
[7] Barnes W L, Kitson S C, Preist T W and Sambles J R 1997 *J. Opt. Soc. Am.* **14** 1654
[8] Mills D L 1977 *Phys. Rev.* B **15** 3097
[9] Lakes B, Mills D L and Maradudin A A 1981 *Phys. Rev.* B **23** 4965
[10] Glass N E, Weber M and Mills D L 1984 *Phys. Rev.* B **29** 6548
[11] Weber M G and Mills D L 1985 *Phys. Rev.* B **31** 2510
[12] Wang S, Barrera R G, and Mochán W L 1989 *Phys. Rev.* B **40** 1571

[13] Cocoletzi G H and Wang S 1993 *Phys. Rev.* B **48** 17 413
[14] Agarwal G S 1977 *Phys. Rev.* B **15** 2371
[15] Elson J M and Ritchie R H 1974 *Phys. Status Solidi* b **62** 461
[16] Chandezon J, Dupuis M T and Cornet G 1982 *J. Opt. Soc. Am.* **72** 839
[17] Halevi P and Guerra-Vela C 1978 *Phys. Rev.* B **18** 5248
[18] Kushwaha M S and Halevi P 1988 *Phys. Rev.* B **38** 12 428
[19] Kushwaha M S and Halevi P 1987 *Solid State Commun.* **64** 1405
[20] Kushwaha M S 1991 *Surf. Sci.* **262** 451
[21] Halevi P 1981 *Phys. Rev.* B **23** 2635
[22] Kushwaha M S 1993 *Phys. Rev.* B **48** 15 445
[23] Albuquerque E L, Fulco P, Farias G A, Auto M M and Tilley D R 1991 *Phys. Rev.* B **43** 2032
[24] Johnson B L and Camley R E 1988 *Phys. Rev.* B **38** 3311
[25] Kushwaha M S 1989 *Phys. Rev.* B **40** 1692
[26] Kushwaha M S 1990 *Phys. Rev.* B **41** 5602
[27] Mochán W L, del Castillo-Mussot M and Barrera R G 1987 *Phys. Rev.* B **35** 1088
[28] Mochán W L and del Castillo-Mussot M 1988 *Phys. Rev.* B **37** 6763
[29] Olazagasti E L, Cocoletzi G H and Mochán W L 1991 *Solid State Commun.* **78** 9
[30] Studies of optical properties of superlattices composed of alternating metallic or highly doped semiconductor layers in the presence of applied external magnetic fields are described in
Martinez G, Jacobo-Escobar J H, Hernández P H and Cocoletzi G H 1999 *Phys. Rev.* B at press
[31] Chiu K W and Quinn J J 1972 *Phys. Rev.* B **5** 4707